

A semiclassical study of the thermal conductivity of low temperature liquids

Jian Liu, Berni J. Alder, and William H. Miller

Citation: *J. Chem. Phys.* **135**, 114105 (2011); doi: 10.1063/1.3639107

View online: <https://doi.org/10.1063/1.3639107>

View Table of Contents: <http://aip.scitation.org/toc/jcp/135/11>

Published by the [American Institute of Physics](#)

Articles you may be interested in

[Path integral Liouville dynamics for thermal equilibrium systems](#)

The Journal of Chemical Physics **140**, 224107 (2014); 10.1063/1.4881518

[Path integral Liouville dynamics: Applications to infrared spectra of OH, water, ammonia, and methane](#)

The Journal of Chemical Physics **144**, 034307 (2016); 10.1063/1.4939953

[Stationary state distribution and efficiency analysis of the Langevin equation via real or virtual dynamics](#)

The Journal of Chemical Physics **147**, 184104 (2017); 10.1063/1.4996204

[Path integral molecular dynamics for exact quantum statistics of multi-electronic-state systems](#)

The Journal of Chemical Physics **148**, 102319 (2018); 10.1063/1.5005059

[An approach for generating trajectory-based dynamics which conserves the canonical distribution in the phase space formulation of quantum mechanics. I. Theories](#)

The Journal of Chemical Physics **134**, 104101 (2011); 10.1063/1.3555273

[A simple model for the treatment of imaginary frequencies in chemical reaction rates and molecular liquids](#)

The Journal of Chemical Physics **131**, 074113 (2009); 10.1063/1.3202438

PHYSICS TODAY

WHITEPAPERS

ADVANCED LIGHT CURE ADHESIVES

Take a closer look at what these environmentally friendly adhesive systems can do

READ NOW

PRESENTED BY
 **MASTERBOND**
ADHESIVES | SEALANTS | COATINGS

A semiclassical study of the thermal conductivity of low temperature liquids

Jian Liu,¹ Berni J. Alder,² and William H. Miller^{1,a)}

¹Department of Chemistry and K. S. Pitzer Center for Theoretical Chemistry, University of California, and Chemical Science Division, Lawrence Berkeley National Laboratory, Berkeley, California 94720-1460, USA

²Lawrence Livermore National Laboratory, Livermore, California 94550, USA

(Received 1 August 2011; accepted 26 August 2011; published online 19 September 2011)

The conventional classical energy current auto-correlation function has been extended into a quantum mechanical version and then approximated by the linearized semiclassical initial value representation approach. Comparison of the thermal conductivity to simulation results shows that about 15% quantum correction to the classical molecular dynamics results for liquid neon are quantitatively predicted. For liquid *para*-hydrogen the quantum effects are sufficiently large that the linearized semiclassical approach is only 20% accurate, while for both liquid He⁴ and He³ the thermal conductivity disagrees by a factor of 2, although exchange effects appear to play a minor role. © 2011 American Institute of Physics. [doi:10.1063/1.3639107]

I. INTRODUCTION

This work is motivated by trying to understand how the energy generated by the fusion reaction is propagated. The critical property required for this process is knowing the thermal conductivity of a plasma of protons and electrons. The fusion reaction, as it takes place at the center of the sun or in a capsule at the National Ignition Facility at Livermore, is under nearly classical conditions since the temperature is so high. Thus, the first approximation for the thermal conductivity is to use the energy current autocorrelation generated from classical molecular dynamics (MD) trajectories with some quantum mechanical cross sections to avoid the coulomb singularities. However, one would like to know how large the quantum corrections to the classical values are; particularly, also at lower temperatures as the plasma cools down. For that purpose the semiclassical (SC) theory^{1,2} is a natural application. Furthermore, one can utilize the classical trajectories.

The simplest (and most approximate) version of the SC initial value representations³ (SC-IVRs) is its “linearized” approximation (LSC-IVR).^{4–6} LSC-IVR can not, for example, describe true quantum coherence effects in time correlation functions, but it does describe a number of aspects of the dynamics very well.^{5,7–17} For example, the LSC-IVR has been shown to describe reactive current correlation functions for chemical reaction rates quite well, including strong tunneling regimes^{4,5,8} and correlation functions^{5,9,11–21} in systems with enough degrees of freedom for quantum re-phasing to be unimportant. (We also note that the forward-backward semiclassical dynamics approximation of Makri *et al.*^{22–27} is very similar to it.) Non-linearized versions of semi-classical theory²⁸ would be more accurate, but are computationally harder to implement.

The purpose of the paper is to present the atomistic/molecular level description of the thermal conductivity

of low temperature liquids to investigate how low temperature quantum dynamical effects can be quantitatively accounted for by this version of the semi-classical theory. Section II first summarizes the relation between thermal correlation functions of the system and experimental observables for dynamical properties and extends the classical version^{29–31} of the energy current auto-correlation function into quantum mechanics. Then Sec. III briefly reviews the LSC-IVR methodology and gives the explicit LSC-IVR formulation for the energy current auto-correlation function investigated in the present study. Section IV presents the LSC-IVR simulation results and compares them to those given by classical MD and also to experimental data. Concluding remarks are given in Sec. V.

II. THERMAL CONDUCTIVITY AND ENERGY CURRENT AUTO-CORRELATION FUNCTION

Most dynamical properties can be expressed in terms of time correlation functions^{30–32}, which are of the form

$$C_{AB}(t) = \frac{1}{Z} \text{Tr}(\hat{A}^\beta e^{i\hat{H}t/\hbar} \hat{B} e^{-i\hat{H}t/\hbar}). \quad (1)$$

Here, $Z = \text{Tr}[e^{-\beta\hat{H}}]$ is the partition function, $\beta = 1/k_B T$ is the inverse temperature, \hat{H} is the (time-independent) Hamiltonian of the system, and \hat{A} and \hat{B} are operators relevant to the specific property of interest. In this paper, we use the Kubo-transformed correlation function³³, i.e., $\hat{A}_{Kubo}^\beta = \frac{1}{\beta} \int_0^\beta d\lambda e^{-(\beta-\lambda)\hat{H}} \hat{A} e^{-\lambda\hat{H}}$ in Eq. (1), as a matter of convenience, as before.^{5,11,13}

The thermal conductivity, λ , measures the rate of heat/energy flow through the system at a given temperature T . It is defined by Fourier’s law of heat conduction:

$$\rho_m c_v \frac{\partial T}{\partial t} = \lambda \nabla^2 T, \quad (2)$$

where c_v is the specific heat and ρ_m is the mass density. Equation (2) is an empirical law based on observation. Based on the “local thermodynamic equilibrium” approximation and

^{a)} Author to whom correspondence should be addressed: Electronic mail: millerwh@berkeley.edu.

the hydrodynamic equations,³⁴ one can show that the thermal conductivity can be expressed in terms of the energy current auto-correlation function.^{29-31,34-36} This definition of the energy current in classical mechanics³⁰ will now be extended into a Hermitian operator of the quantum mechanical correlation function, as follows.

Suppose that the system consists of N particles and only pair-wise interactions are involved, i.e., the Hamiltonian is

$$\hat{H} = \sum_{j=1}^N \frac{\hat{\mathbf{p}}_j^2}{2m_j} + \frac{1}{2} \sum_{j=1}^N \sum_{\substack{k=1 \\ k \neq j}}^N \hat{V}(r_{jk}). \quad (3)$$

The thermal conductivity λ of the one-component system can be obtained from the energy current autocorrelation function

$$\lambda = \frac{1}{3Vk_B T^2} \int_0^\infty \langle \hat{\mathbf{S}}(0) \cdot \hat{\mathbf{S}}(t) \rangle dt, \quad (4)$$

where V is the volume of the system.^{29-31,34-36} The energy current of the system is defined as

$$\hat{\mathbf{S}} = \frac{d}{dt} \hat{\mathbf{G}} \equiv \hat{\mathbf{G}}, \quad (5)$$

where

$$\hat{\mathbf{G}} = \frac{1}{2} \sum_{j=1}^N \left[\hat{\mathbf{r}}_j \left(\frac{\hat{\mathbf{p}}_j^2}{2m_j} + \frac{1}{2} \sum_{\substack{k=1 \\ j \neq k}}^N \hat{V}(r_{jk}) \right) + \left(\frac{\hat{\mathbf{p}}_j^2}{2m_j} + \frac{1}{2} \sum_{\substack{k=1 \\ j \neq k}}^N \hat{V}(r_{jk}) \right) \hat{\mathbf{r}}_j \right]. \quad (6)$$

As discussed in Appendix A, one can rigorously prove that the Hermitian operator of Eq. (5) can be expressed in quantum mechanics as

$$\begin{aligned} \hat{\mathbf{S}} &= \frac{1}{i\hbar} [\hat{\mathbf{G}}, \hat{H}] \\ &= \sum_{j=1}^N \frac{1}{2} \left(\frac{\hat{\mathbf{p}}_j}{m_j} \frac{\hat{\mathbf{p}}_j^2}{2m_j} + \frac{\hat{\mathbf{p}}_j^2}{2m_j} \frac{\hat{\mathbf{p}}_j}{m_j} \right) \\ &\quad + \frac{1}{4} \sum_{j=1}^N \sum_{\substack{k=1 \\ k \neq j}}^N \left(\frac{\hat{\mathbf{p}}_j}{m_j} \hat{V}(r_{kj}) + \hat{V}(r_{kj}) \frac{\hat{\mathbf{p}}_j}{m_j} \right) \\ &\quad - \frac{1}{4} \sum_{j=1}^N \sum_{\substack{k=1 \\ k \neq j}}^N \left\{ \hat{\mathbf{r}}_{kj} \left[\frac{\partial \hat{V}(r_{kj})}{\partial \mathbf{r}_{kj}} \cdot \frac{\hat{\mathbf{p}}_j}{2m_j} + \frac{\hat{\mathbf{p}}_j}{2m_j} \cdot \frac{\partial \hat{V}(r_{kj})}{\partial \mathbf{r}_{kj}} \right] \right. \\ &\quad \left. + \left[\frac{\partial \hat{V}(r_{kj})}{\partial \mathbf{r}_{kj}} \cdot \frac{\hat{\mathbf{p}}_j}{2m_j} + \frac{\hat{\mathbf{p}}_j}{2m_j} \cdot \frac{\partial \hat{V}(r_{kj})}{\partial \mathbf{r}_{kj}} \right] \hat{\mathbf{r}}_{kj} \right\}. \quad (7) \end{aligned}$$

The classical correspondence of operator $\hat{\mathbf{S}}$ is simply given by

$$\begin{aligned} \mathbf{S}_{cl} &= \sum_{j=1}^N \frac{\mathbf{p}_j}{m_j} \frac{\mathbf{p}_j^2}{2m_j} + \frac{1}{2} \sum_{j=1}^N \sum_{\substack{k=1 \\ k \neq j}}^N \frac{\mathbf{p}_j}{m_j} V(r_{kj}) \\ &\quad - \frac{1}{2} \sum_{j=1}^N \sum_{\substack{k=1 \\ k \neq j}}^N \mathbf{r}_{kj} \frac{\partial V(r_{kj})}{\partial \mathbf{r}_{kj}} \cdot \frac{\mathbf{p}_j}{m_j}. \quad (8) \end{aligned}$$

In principle, one can also express the thermal conductivity by the Einstein-Kubo-Helfand^{37,38} relation. However, this approach is ambiguous for finite systems subject to periodic boundary conditions.³⁹ Hence, we use the Green-Kubo approach^{36,37,40} as represented by Eq. (4).

It is sometimes useful to directly compare the integral of the autocorrelation function,

$$\frac{1}{3N} \int_0^\infty \langle \hat{\mathbf{S}}(0) \cdot \hat{\mathbf{S}}(t) \rangle dt = \frac{\lambda k_B T^2}{\rho}, \quad (9)$$

to experiments,⁴¹ rather than the thermal conductivity itself. Here, $\rho = N/V$ is the number density. The energy current (Eq. (7)) is not a single particle quantity but represents a collective property for all the molecules/particles of the system [similar to the collective dipole (or dipole-derivative) auto-correlation function for the infrared spectrum of liquid water^{17,42}]. The time-dependence of the auto-correlation function for the thermal conductivity can help gain insight into the nature on how heat/energy is transported as a collective behavior and its integral compared to the experiment provides a good test for the methodology on the description of quantum effects in dynamical properties.

III. SIMULATION METHODOLOGY

A. Linearized semiclassical initial value representation

The SC-IVR approximates the forward (backward) time evolution operator $e^{-i\hat{H}t/\hbar}$ ($e^{i\hat{H}t/\hbar}$) by a phase space average over the initial conditions of forward (backward) classical trajectories.^{1,28} By making the approximation that the dominant contribution to the phase space averages comes from forward and backward trajectories that are infinitesimally close to one another, and then linearizing the difference between the forward and backward actions (and other quantities in the integrand), Wang, Sun, and Miller^{4,7} (see also Ref. 14) obtained the LSC-IVR, or classical Wigner model for the correlation function in Eq. (1),

$$\begin{aligned} C_{AB}^{\text{LSC-IVR}}(t) &= Z^{-1} (2\pi\hbar)^{-3N} \int d\mathbf{x}_0 \\ &\quad \times \int d\mathbf{p}_0 A_w^\beta(\mathbf{x}_0, \mathbf{p}_0) B_w(\mathbf{x}_t, \mathbf{p}_t), \quad (10) \end{aligned}$$

where A_w^β and B_w are the Wigner functions⁴³ corresponding to these operators,

$$O_w(\mathbf{x}, \mathbf{p}) = \int d\Delta x \left\langle \mathbf{x} - \frac{\Delta x}{2} \left| \hat{O} \right| \mathbf{x} + \frac{\Delta x}{2} \right\rangle e^{i\mathbf{p}^T \Delta x / \hbar}, \quad (11)$$

for any operator \hat{O} . Here, $(\mathbf{x}_0, \mathbf{p}_0)$ is the set of initial coordinates and momenta for a classical trajectory, $(\mathbf{x}_t(\mathbf{x}_0, \mathbf{p}_0), \mathbf{p}_t(\mathbf{x}_0, \mathbf{p}_0))$ being the phase point at time t along this trajectory.

The classical Wigner model is an old idea,⁴³⁻⁴⁶ but it is informative to realize that it is contained within the general SC-IVR formulation, namely, as a specific approximation to it;^{4,7} more accurate implementations of the SC-IVR approach would be expected to lead to a more accurate description. It should also be noted that there are other

approximate routes^{6,10,47,48} which lead to the classical Wigner model for correlation functions other than simply postulating it (see more discussion in Ref. 5). Moreover, two of us^{10,49} have recently shown that the exact quantum time correlation function can be expressed in the same form as Eq. (10), with an associated dynamics in the single phase space, and it was furthermore demonstrated that the LSC-IVR correctly leads to the classical limit ($\hbar \rightarrow 0$), high temperature limit ($\beta \rightarrow 0$), and harmonic limit.

B. Explicit formulations

Calculation of the Wigner function for operator \hat{B} in Eq. (10) is usually straightforward; in fact, \hat{B} is often a function only of coordinates or only of momenta, in which case its Wigner function is simply the classical function itself. It is further shown in Appendix B that the Wigner function for such an operator as the energy current operator \hat{S} is the same as the classical formula. That is,

$$S_W \equiv [\hat{S}]_W = \sum_{j=1}^N \frac{\mathbf{p}_j}{m_j} \frac{\mathbf{p}_j^2}{2m_j} + \frac{1}{2} \sum_{j=1}^N \sum_{\substack{k=1 \\ k \neq j}}^N \frac{\mathbf{p}_j}{m_j} V(r_{kj}) - \frac{1}{2} \sum_{j=1}^N \sum_{\substack{k=1 \\ k \neq j}}^N \mathbf{r}_{kj} \frac{\partial V(r_{kj})}{\partial \mathbf{r}_{kj}} \cdot \frac{\mathbf{p}_j}{m_j}. \quad (12)$$

Calculating the Wigner function for operator \hat{A}^β , however, involves the Boltzmann operator with the total Hamiltonian of the entire system, so that carrying out the multidimensional Fourier transform to obtain it is far from trivial. To accomplish this task, the local Gaussian approximation⁵ and several other approximations^{4,9,14,48} have been introduced. Here, such a further simplifying approximation is introduced to obtain the Wigner function for the operator $\hat{S}_{Kubo}(\hat{A}^\beta)$, because the energy current operator \hat{S} (Eq. (7)) is a very complex function of both $\hat{\mathbf{x}}$ and $\hat{\mathbf{p}}$.

By virtue of our recent work (i.e., Eq. (18) and Eqs. (62)–(70) of Ref. 50), one can express the Wigner function for the Boltzmann operator $e^{-\beta \hat{H}}$ as

$$\frac{1}{Z} [e^{-\beta \hat{H}}]_W(\mathbf{x}, \mathbf{p}) \approx \frac{1}{Z} \left(\frac{\beta}{2\pi} \right)^{3N/2} \det(\mathbf{M})^{-1} e^{-\frac{\beta}{2} \mathbf{p}^T \mathbf{M}^{-1} \mathbf{p}} P_c(\mathbf{x}), \quad (13)$$

with the (diagonal) mass matrix, \mathbf{M} , the centroid variable

$$\mathbf{x}_c = \frac{1}{P} (\mathbf{x}_1 + \mathbf{x}_2 + \cdots + \mathbf{x}_P), \quad (14)$$

and the centroid density

$$P_c(\mathbf{x}) = \lim_{P \rightarrow \infty} \left(\frac{P}{2\pi\beta\hbar^2} \right)^{3NP/2} |\mathbf{M}|^{P/2} \int d\mathbf{x}_1 \cdots \int d\mathbf{x}_P \delta(\mathbf{x} - \mathbf{x}_c) \times \exp \left\{ -\frac{P}{2\beta\hbar^2} [(\mathbf{x}_1 - \mathbf{x}_2)^T \mathbf{M}(\mathbf{x}_1 - \mathbf{x}_2) + \cdots + (\mathbf{x}_P - \mathbf{x}_1)^T \mathbf{M}(\mathbf{x}_P - \mathbf{x}_1)] \right\} \times \exp \left\{ -\frac{\beta}{P} [V(\mathbf{x}_1) + \cdots + V(\mathbf{x}_P)] \right\}, \quad (15)$$

which yields the partition function

$$Z = \int d\mathbf{x} P_c(\mathbf{x}). \quad (16)$$

Here, P is the number of path integral beads.

Similarly, one can approximately express the Wigner function for operator \hat{S}_{Kubo} as

$$[\hat{S}_{Kubo}]_W(\mathbf{x}, \mathbf{p}) \approx \left(\frac{\beta}{2\pi} \right)^{3N/2} \det(\mathbf{M})^{-1} e^{-\frac{\beta}{2} \mathbf{p}^T \mathbf{M}^{-1} \mathbf{p}} \times P_c(\mathbf{x}) S_W(\mathbf{x}, \mathbf{p}). \quad (17)$$

By virtue of Eq. (10), the explicit form of the LSC-IVR approximation to $\langle \hat{S}(0) \cdot \hat{S}(t) \rangle_{Kubo}$ is thus given by

$$\langle \hat{S}(0) \cdot \hat{S}(t) \rangle_{Kubo}^{LSC-IVR} \approx \frac{1}{Z} \int d\mathbf{x}_0 \int d\mathbf{p}_0 \left(\frac{\beta}{2\pi} \right)^{3N/2} \times \det(\mathbf{M})^{-1} e^{-\frac{\beta}{2} \mathbf{p}_0^T \mathbf{M}^{-1} \mathbf{p}_0} P_c(\mathbf{x}_0) \times \mathbf{S}_W(\mathbf{x}_0, \mathbf{p}_0) \cdot \mathbf{S}_W(\mathbf{x}_t, \mathbf{p}_t). \quad (18)$$

[Also see the note in Ref. 51.]

For comparison, the classical energy current correlation function is simply given by $\langle \mathbf{S}_{cl}(\mathbf{x}_0, \mathbf{p}_0) \cdot \mathbf{S}_{cl}(\mathbf{x}_t, \mathbf{p}_t) \rangle$ with the bracket representing the classical canonical ensemble average.²⁹

IV. RESULTS AND DISCUSSIONS

A. Simulation details

Given the interaction between particles of the system, both classical MD and LSC-IVR are able to provide the microscopic simulation for macroscopic dynamical properties, without any additional fitting parameters or models. In this paper, we focus on the thermal conductivity of liquids consisted of light molecules (neon, *para*-hydrogen, He⁴ or He³) in a range of temperature, where quantum effects are expected to be non-negligible and experiments are available.

We use the most recent *ab initio* based potential energy surface⁵² for the interaction between neon atoms. The triple point temperature of liquid neon is $T = 24.556$ K and the critical point temperature is $T = 44.4$ K. Because the mass of neon is relatively heavy, one expects that quantum effects in liquid neon are not prominent if the temperature is not low. So, we compare the thermal conductivity of liquid neon at two state points along the saturated line near its triple point^{53,54} $T = 28$ K, $\rho_m = 1189$ kg m⁻³, $p_{sat} = 1.321$ bars, and $T = 26$ K, $\rho_m = 1224$ kg m⁻³, $p_{sat} = 0.7184$ bar with the experimental data.⁵³

The interaction between molecules in liquid *para*-hydrogen is well described by the Silvera-Goldman model.⁵⁵ Liquid *para*-hydrogen has previously served as a benchmark system to test LSC-IVR (Refs. 5, 11, and 12) and its maximum entropy analytical continuation correction.^{5,13} The triple point temperature of *para*-hydrogen is 13.8 K and the critical temperature is $T_c \approx 33.1$ K. As given in Refs. 5, 11–13, 56, and 57, we investigate the four state points under nearly zero external pressure, $T = 25$ K, $v = 31.7$ cm³ mol⁻¹, $T = 20$ K, $v = 28.1$ cm³ mol⁻¹, $T = 17$ K,

TABLE I. The thermal conductivity of liquid *para*-hydrogen (see more simulation data in Fig. 3).

T (K)	ρ_m (kg/m ³)	λ (Js ⁻¹ m ⁻¹ K ⁻¹)		Experiment (Ref. 59)
		LSC-IVR	Classical	
16.942	74.556	0.0918 ± 0.0042	0.1801 ± 0.0075	0.0942
19.522	71.799	0.0983
22.001	69.066	0.0842 ± 0.0032	0.1600 ± 0.0057	0.1019
24.990	64.916	0.0817 ± 0.0034	0.1476 ± 0.0069	0.1013
30.026	56.361	0.0742 ± 0.0027	0.1239 ± 0.0035	0.0915
33.001	45.900	0.0840

$v = 26.9$ cm³mol⁻¹, and $T = 14$ K, $v = 25.6$ cm³mol⁻¹. ($v = 1/\rho$ is the molar volume.) In addition, we study three more state points along the saturation line,⁵⁸ $T = 30$ K, $\rho_m = 53.9112$ kgm⁻³, $T = 27$ K, $\rho_m = 60.9628$ kgm⁻³, and $T = 22$ K, $\rho_m = 68.7600$ kgm⁻³. The measurements by Roder and Diller⁵⁹ appear to be most accurate⁶⁰ (with about 7.79% average deviation⁶⁰), which provide six state points (as shown in Fig. 3 and Table I) close to those in our simulations.

Liquid He⁴ and liquid He³ are described by the HFD-B2 potential given by Aziz *et al.*⁶¹ The critical point temperature of liquid He⁴ is 5.2 K and the superfluid λ -transition-point temperature is 2.17 K; the critical point temperature of liquid He³ is 3.31 K. We consider two state points at the saturated vapor pressure⁶² at $T = 3$ and 4 K of liquid He⁴ and one near the saturated vapor pressure^{63,64} at $T = 3$ K of liquid He³. The thermal de Broglie wavelengths ($\Lambda = h/\sqrt{2\pi mk_B T}$) in normal liquid He⁴ at $T = 4$ and 3 K are about 4.35 Å and 5.02 Å, respectively. They are slightly larger than the average distance $\rho^{-1/3}$ between particles of the two state points (3.73 Å and 3.62 Å, respectively). Similarly, the thermal de Broglie wavelength in normal liquid He³ at $T = 3$ K is about 5.80 Å while the average distance of the state point is 4.27 Å. Since the two length scales are comparable, one expects quantum exchange will exist but not have an enormous effect on the properties of these normal liquid state points. So quantum exchange is ignored in the LSC-IVR simulations.

The bisection method⁶⁵ of the path integral Monte Carlo (PIMC) is implemented to obtain the quantum equilibrium structures of the molecular liquids. The simulation is carried out with a total of 216 molecules in a box with the periodic boundary condition. $P = 8$ beads are used for liquid neon at 26–28 K, $P = 32$ beads are used for the state point of liquid *para*-hydrogen at 25–30 K, $P = 64$ beads for that at 14–22 K, and $P = 128$ beads for liquid He⁴ at 3–4 K, and liquid He³ at 3 K. After systems are equilibrated by PIMC, an initial configuration is produced every $2P + 1$ PIMC steps and the Gaussian distribution in Eq. (18) is used to randomly generate the initial momenta to run a classical trajectory for evaluating the quantity $\mathbf{S}_W(\mathbf{x}_0, \mathbf{p}_0) \cdot \mathbf{S}_W(\mathbf{x}_t, \mathbf{p}_t)$. The time step of the classical trajectory is ~ 1.2 fs and the velocity Verlet algorithm is used in the classical propagation up to 2.5 ps for liquid neon and liquid *para*-hydrogen and up to 14 ps for normal liquid helium. Sum the property $\mathbf{S}_W(\mathbf{x}_0, \mathbf{p}_0) \cdot \mathbf{S}_W(\mathbf{x}_t, \mathbf{p}_t)$ for all real time classical trajectories to obtain a well converged result for the Kubo-transformed energy current auto-

correlation function. About 2.4×10^5 such classical trajectories are used for liquid neon and for liquid *para*-hydrogen, while about 2.4×10^6 such classical trajectories for liquid He⁴ and liquid He³. For comparison, we also run classical simulations for such liquid systems. Because some classical systems at low temperature fall into the meta-stable amorphous solid regime occasionally, Monte Carlo (MC) is used to equilibrate the classical systems to sample initial conditions. We then run short time classical trajectories from those initial conditions and sum the property $\mathbf{S}_{cl}(\mathbf{x}_0, \mathbf{p}_0) \cdot \mathbf{S}_{cl}(\mathbf{x}_t, \mathbf{p}_t)$ to evaluate the energy current correlation function, in a similar way as for LSC-IVR. About 2.4×10^5 such classical trajectories are used for each system. 20 blocks are used in each simulation to obtain the error bar.

B. Results and discussions

While the classical average kinetic energy is only $\langle \hat{\mathbf{p}}^2/2mNk_B \rangle = 39.0$ K at the state point $T = 26$ K for liquid neon, PIMC gives an over 25% larger value 50.41 ± 0.15 K. One, thus, expects quantum effects in the thermal conductivity to be also most noticeable near its triple point. Figure 1 shows comparison of the LSC-IVR energy current auto-correlation function to the classical one for liquid neon at $T = 26$ K. Both LSC-IVR and classical results demonstrate a monotonic decay, damping to zero after 1 ps. One inevitably observes such monotonic decay of the energy current auto-correlation in the pure liquid phase, irrespective of the temperature or density of the system. One also sees from Fig. 1 that the LSC-IVR energy current auto-correlation function shows a slightly slower relaxation than the classical one. For example, the LSC-IVR and classical results yield 0.255 ± 0.002 ps and 0.247 ± 0.002 ps, respectively, for the relaxation time τ at $T = 26$ K. The thermal fluctuations of the energy in quantum mechanics are smaller than that in classical mechanics, (e.g., the specific heat c_v in quantum mechanics is smaller than that in classical mechanics), which makes the relaxation time longer. The thermal conductivity λ and the re-

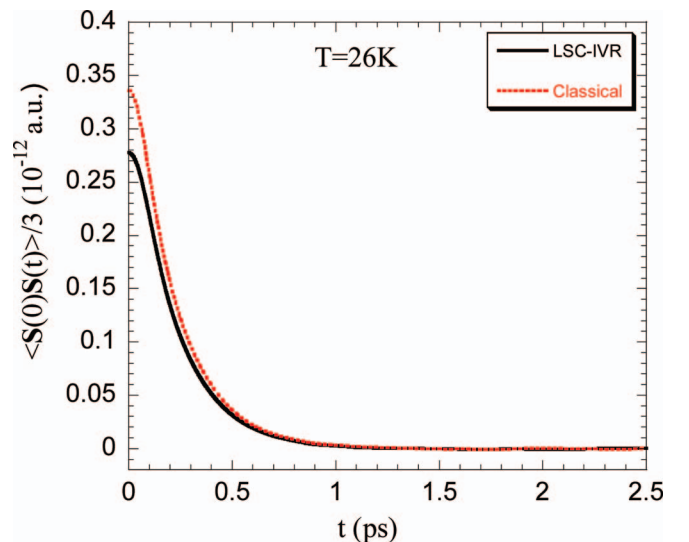


FIG. 1. The energy current autocorrelation functions $\langle \hat{\mathbf{S}}(0) \cdot \hat{\mathbf{S}}(t) \rangle / 3$ for liquid neon at $T = 25$ K.

TABLE II. The thermal conductivity of liquid neon.

	T (K)	ρ_m (kg/m ³)	LSC-IVR	Classical	Experiment (Ref. 53)
λ (Js ⁻¹ m ⁻¹ K ⁻¹)	28.0	1189	0.109 ± 0.005	0.128 ± 0.003	0.112
	26.0	1224	0.115 ± 0.005	0.136 ± 0.002	0.117
$\lambda k_B T^2 / \rho$ (10 ⁻⁵⁰ J ² m ² s ⁻¹)	28.0	1189	3.31 ± 0.17	3.89 ± 0.08	3.42
	26.0	1224	2.94 ± 0.14	3.49 ± 0.06	2.99

lated property $\lambda k_B T^2 / \rho$ are given in Table II. Classical simulations overestimate the thermal conductivity by ~15%. LSC-IVR is able to quantitatively account for the quantum effects as shown by the agreement with the experimental data,⁵³ and its temperature dependence. [Also see the note in Ref. 66.]

Figure 2 shows the LSC-IVR and classical energy current correlation functions of liquid *para*-hydrogen at the two state points at 32 K and 14 K. Both the LSC-IVR and classical results show that the time scale of relaxation in the energy current auto-correlation function increases as the temper-

ature decreased. For instance, LSC-IVR produces $\tau = 0.154 \pm 0.001$ ps at 32 K and $\tau = 0.159 \pm 0.001$ ps at 14 K, while classical MD yields $\tau = 0.100 \pm 0.001$ ps at 32 K and $\tau = 0.112 \pm 0.001$ ps at 25 K, in agreement with the expectation that the magnitude of the fluctuations increase as the temperature increases. The difference between the LSC-IVR and classical results for liquid *para*-hydrogen can be observed to be more prominent than that for liquid neon. Figure 2 also demonstrates that the difference between the LSC-IVR and classical results are more pronounced as the temperature

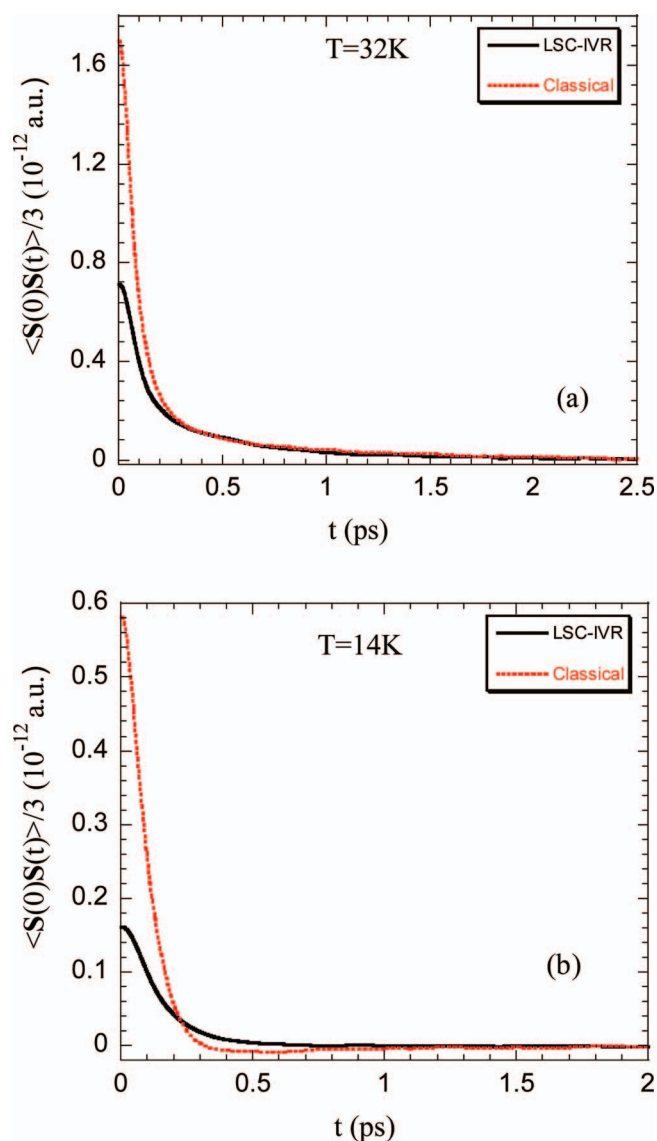


FIG. 2. The energy current autocorrelation functions $\langle \hat{S}(0) \cdot \hat{S}(t) \rangle / 3$ for liquid *para*-hydrogen at $T = 14$ –32 K.

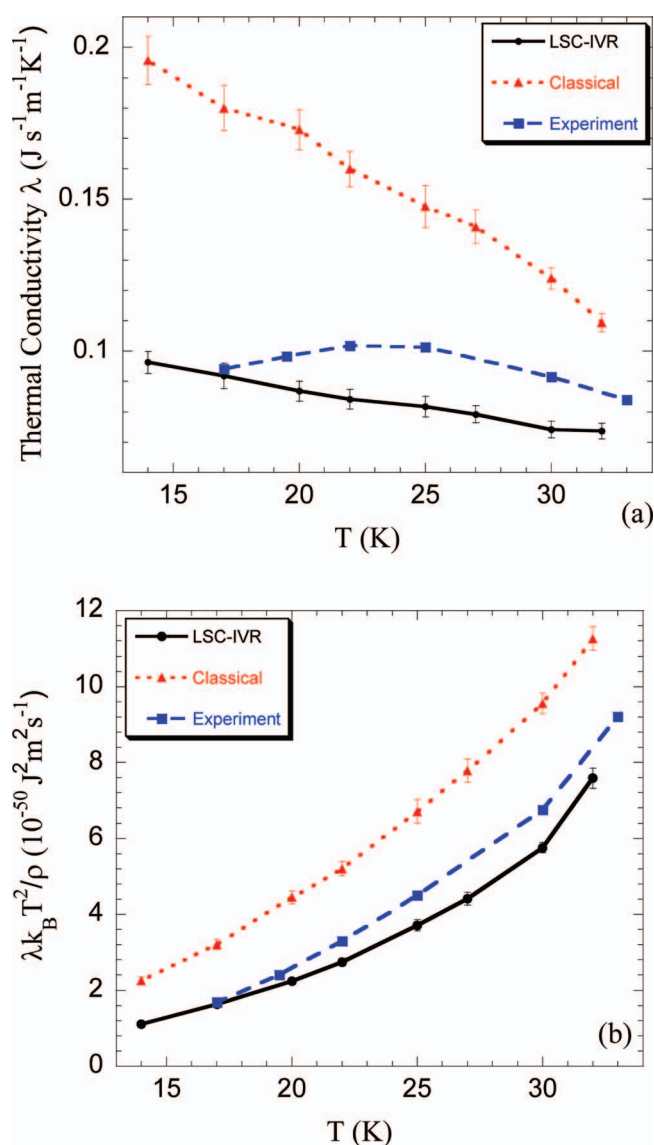


FIG. 3. (a) The thermal conductivity for liquid *para*-hydrogen at $T = 14$ –32 K. (b) Related properties $\lambda k_B T^2 / \rho$.

decreases. As expected, quantum dynamical effects become more prominent as the particle gets lighter and as the temperature decreases. The thermal conductivity is plotted as a function of temperature in Fig. 3. Although the experimental data do not suggest a simple relation between the thermal conductivity λ and the temperature T , they do show that the related property $\lambda k_B T^2 / \rho$ increases monotonically as the temperature is raised, in agreement with both LSC-IVR and classical simulations. Figure 3 shows that the LSC-IVR results significantly improve over the classical results for the thermal conductivity. While the classical simulations can deviate by as much as a factor of 2, less than 20% discrepancy exists between the LSC-IVR results and the experimental data.

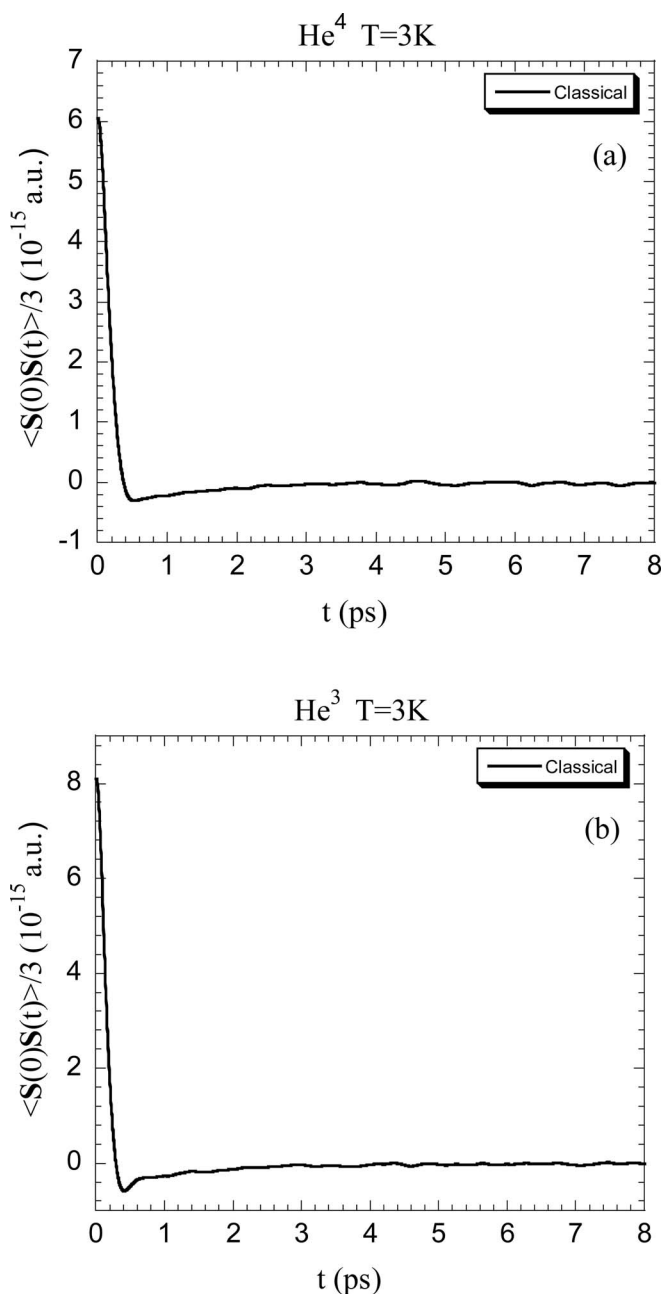


FIG. 4. Classical energy current autocorrelation functions $\langle \hat{S}(0) \cdot \hat{S}(t) \rangle / 3$ (a) for liquid He^4 at $T = 3$ K, and (b) for liquid He^3 at $T = 3$ K.

TABLE III. The thermal conductivity of liquid He^4 .

T (K)	ρ_m (kg/m ³)	λ (10 ⁻² Js ⁻¹ m ⁻¹ K ⁻¹)		$\lambda k_B T^2 / \rho$ (10 ⁻⁵² J ² m ² s ⁻¹)	
		LSC-IVR	Experiment (Ref. 62)	LSC-IVR	Experiment (Ref. 62)
4.0	128.9745	3.96 ± 0.13	1.98	4.54 ± 0.15	2.27
3.0	141.2269	4.50 ± 0.24	1.74	2.65 ± 0.14	1.03

Note that the classical energy current auto-correlation function of liquid *para*-hydrogen at $T = 14$ K becomes negative with a small value after 0.25 ps and stays negative, going to zero at about $t = 1.5$ ps. Such negative values implies back scattering, a typical signature of amorphous solid,^{67,68}

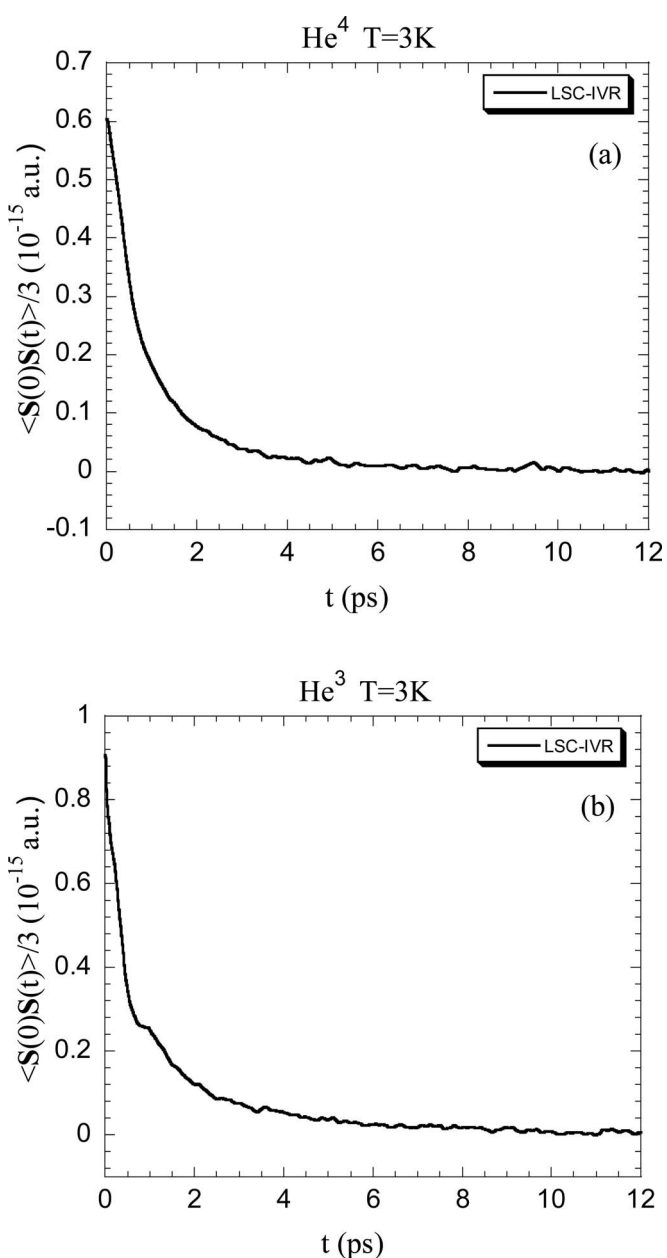


FIG. 5. LSC-IVR energy current autocorrelation functions $\langle \hat{S}(0) \cdot \hat{S}(t) \rangle / 3$ (a) for liquid He^4 at $T = 3$ K and (b) for liquid He^3 at $T = 3$ K.

TABLE IV. The thermal conductivity of liquid He³.

T (K)	ρ_m (kg/m ³)	λ (10 ⁻² Js ⁻¹ m ⁻¹ K ⁻¹)		$\lambda k_B T^2/\rho$ (10 ⁻⁵² J ² m ² s ⁻¹)	
		LSC-IVR	Experiment (Ref. 64)	LSC-IVR	Experiment (Ref. 64)
3.0	64.574 ⁶³	4.10 ± 0.20	1.69	3.96 ± 0.19	~1.63

because the heat energy carried by phonons are reflected back. Classical simulation show that at lower temperatures, the liquid systems fall into the metastable amorphous solid regime and thereby gives a qualitatively wrong microscopic physical picture. This is exactly what Fig. 4 demonstrates for the classical energy current auto-correlation functions of liquid He⁴ and of liquid He³ at 3 K. One sees that the correlation function reaches even pronounced negative value around 0.4 ps followed by a long negative tail.

In contrast, Fig. 5 shows the LSC-IVR energy current auto-correlation functions of the liquid helium systems. All the correlation functions show a monotonic decay to zero, a typical picture for heat transport in the liquid phase. The substantial difference between the classical and LSC-IVR energy current auto-correlation functions is attributed to zero point energy effects, which make the molecules in these low temperature (3–4 K) systems much more mobile to stay in the liquid state rather than the amorphous solid state. Quantum effects are large, for instance, the average kinetic energy ($\langle \hat{\mathbf{p}}^2/2mNk_b \rangle$) is ~ 15.96 K for liquid He⁴ at $T = 3$ K, more than three times of the classical result 4.5 K. The thermal conductivity λ and the related property $\lambda k_B T^2/\rho$ of these systems are listed in Tables III and IV. While classical MD totally misses the correct physical picture [so it is meaningless to obtain the integral of the correlation function], LSC-IVR is qualitatively correct but overestimates the thermal conductivity by a factor of ~ 2 in the normal liquid He⁴ or He³ systems. LSC-IVR calculations also show $\lambda k_B T^2/\rho$ decreases as the temperature decreases for liquid He⁴, which agrees with the experimental data. However, LSC-IVR suggests that the thermal conductivity increases as the temperature decreases, inconsistent with the experimental data.

The discrepancy between LSC-IVR and experimental results appear not be due to quantum exchange. Although He⁴ particles are bosons and He³ atoms are fermions, the ratio of the thermal conductivity of liquid He⁴ to that of liquid He³ at the temperature 3 K is given by LSC-IVR ~ 1.098 while the experimental data gives the ratio $\lambda_{He^4}/\lambda_{He^3} \approx 1.030$. These ratios close to one imply that quantum exchange effects are not very important in the thermal conductivity in normal liquid He⁴ and He³ even at 3 K.

The approximation of real time dynamics in LSC-IVR instead is very likely the major source for the discrepancy. Figure 5 demonstrates the relaxation times of the energy current auto-correlation functions for liquid He⁴ and He³ are much longer than those for liquid *para*-hydrogen and liquid neon. LSC-IVR is a good short time approximation to quantum dynamics and is less adequate for accurately describing long time behavior of the correlation function.^{5,10,12,26,49,50} More accurate SC-IVR approaches²⁸ are needed for more faithful description on long time quantum dynamical effects,

which involve more computational efforts. In addition, several more approaches^{10,13,49,50,69} have been recently proposed to improve over LSC-IVR at longer time and lower temperature in a single phase space. It will be interesting to apply them to study the thermal conductivity in the future.

V. CONCLUSIONS

In this paper, we have applied the LSC-IVR method to study quantum dynamical effects in the thermal conductivity in light molecular liquids. The conventional classical version^{29–31} of the energy current auto-correlation function has been extended into a quantum mechanical version and then approximated by LSC-IVR with centroid coordinates—an approximate semiclassical approach to account for quantum dynamical effects. The good agreement between experimental data and LSC-IVR simulations of the thermal conductivity for liquid neon shows that LSC-IVR is a good short time approximation for treating quantum correlation functions, as was demonstrated before. In molecular liquids with lighter particles and lower temperatures, i.e., liquid *para*-hydrogen and at even lower temperatures normal liquid He⁴ and He³, this linearized semiclassical approach is progressively less adequate, however, qualitatively, the related quantity $\lambda k_B T^2/\rho$ increases as the temperature increases, in agreement with the experiment. One can also demonstrate that for the two isotopes of helium the exchange effects, which have been ignored in our current study, are not quantitatively significant, although they could have been included in the Feynman path integral implementation of LSC-IVR. More advanced versions of SC-IVRs²⁸ would no doubt lead to better agreement with experiment, but require much computational effort. For the moment, the LSC-IVR model employed here seems adequate for the plasma fusion application, since quantum effects are expected to be small under fusion conditions. For the plasma calculation the additional complication is that we need to deal with a two-component system of vastly different masses.

ACKNOWLEDGMENTS

This work was supported by the National Science Foundation (NSF) Grant No. CHE-0809073 and by the Director, Office of Science, Office of Basic Energy Sciences, Chemical Sciences, Geosciences, and Biosciences Division, U.S. Department of Energy (DOE) under Contract No. DE-AC02-05CH11231. We acknowledge a generous allocation of supercomputing time from the National Energy Research Scientific Computing Center (NERSC) and the use of the Lawrence computational cluster resource provided by the IT Division at the Lawrence Berkeley National Laboratory. The work is also

supported by the 2011 NERSC initiative for scientific exploration award.

APPENDIX A: EXPRESSION OF THE ENERGY CURRENT OPERATOR \hat{S}

Here, we derive the quantum mechanical energy current operator \hat{S} (i.e., Eq. (7)) from the definition of the operator \hat{G} (i.e., Eq. (6)).

From the following commutation relations:

$$[\hat{x}_j, \hat{p}_n] = i\hbar\delta_{jn}, \quad (\text{A1})$$

$$[\hat{A}, \hat{B}\hat{C}] = [\hat{A}, \hat{B}]\hat{C} + \hat{B}[\hat{A}, \hat{C}], \quad (\text{A2})$$

and

$$[f(\hat{x}_j), \hat{p}_n] = i\hbar\delta_{jn}f'(\hat{x}_j), \quad (\text{A3}) \quad \text{and}$$

it is straightforward to show

$$\left[\hat{\mathbf{r}}_j, \frac{\hat{\mathbf{p}}_n^2}{2m_n} \right] = i\hbar\delta_{jn} \frac{\hat{\mathbf{p}}_n}{2m_n} \quad (\text{A4})$$

and

$$[\hat{\mathbf{p}}_j, \hat{V}(r_{kn})] = -i\hbar\delta_{jk} \frac{\partial \hat{V}(r_{kn})}{\partial \mathbf{r}_{kn}} + i\hbar\delta_{jn} \frac{\partial \hat{V}(r_{kn})}{\partial \mathbf{r}_{kn}}. \quad (\text{A5})$$

Here, $\hat{\mathbf{r}}_j$ and $\hat{\mathbf{p}}_j$ are the position and the momentum operators of the j th particle, and m_j is the mass of the j th particle. r_{jk} is the distance between the j th and k th particles with the vector operator $\hat{\mathbf{r}}_{jk} = \hat{\mathbf{r}}_j - \hat{\mathbf{r}}_k$. It is easy to further show

$$\begin{aligned} \left[\sum_{j=1}^N \hat{\mathbf{r}}_j \frac{\hat{\mathbf{p}}_j^2}{2m_j}, \sum_{n=1}^N \frac{\hat{\mathbf{p}}_n^2}{2m_n} \right] &= \sum_{j=1}^N \left[\hat{\mathbf{r}}_j, \sum_{n=1}^N \frac{\hat{\mathbf{p}}_n^2}{2m_n} \right] \frac{\hat{\mathbf{p}}_j^2}{2m_j} \\ &= i\hbar \sum_{j=1}^N \frac{\hat{\mathbf{p}}_j}{m_j} \frac{\hat{\mathbf{p}}_j^2}{2m_j} \end{aligned} \quad (\text{A6})$$

$$\begin{aligned} \left[\hat{\mathbf{r}}_j \frac{1}{2} \sum_{\substack{k=1 \\ k \neq j}}^N \hat{V}(r_{kj}), \sum_{n=1}^N \frac{\hat{\mathbf{p}}_n^2}{2m_n} \right] &= \left[\hat{\mathbf{r}}_j, \sum_{n=1}^N \frac{\hat{\mathbf{p}}_n^2}{2m_n} \right] \frac{1}{2} \sum_{\substack{k=1 \\ k \neq j}}^N \hat{V}(r_{kj}) + \hat{\mathbf{r}}_j \sum_{n=1}^N \left[\frac{1}{2} \sum_{\substack{k=1 \\ k \neq j}}^N \hat{V}(r_{kj}), \frac{\hat{\mathbf{p}}_n^2}{2m_n} \right] \\ &= i\hbar \frac{1}{2} \frac{\hat{\mathbf{p}}_j}{m_j} \sum_{\substack{k=1 \\ k \neq j}}^N \hat{V}(r_{kj}) - i\hbar \hat{\mathbf{r}}_j \frac{1}{2} \sum_{\substack{k=1 \\ k \neq j}}^N \left[\frac{\partial \hat{V}(r_{kj})}{\partial \mathbf{r}_{kj}} \cdot \frac{\hat{\mathbf{p}}_j}{2m_j} + \frac{\hat{\mathbf{p}}_j}{2m_j} \cdot \frac{\partial \hat{V}(r_{kj})}{\partial \mathbf{r}_{kj}} \right] \\ &\quad + i\hbar \hat{\mathbf{r}}_j \frac{1}{2} \sum_{\substack{n=1 \\ n \neq j}}^N \left[\frac{\partial \hat{V}(r_{nj})}{\partial \mathbf{r}_{nj}} \cdot \frac{\hat{\mathbf{p}}_n}{2m_n} + \frac{\hat{\mathbf{p}}_n}{2m_n} \cdot \frac{\partial \hat{V}(r_{nj})}{\partial \mathbf{r}_{nj}} \right]. \end{aligned} \quad (\text{A7})$$

Taking the summation over j on both sides of Eq. (A7), replacing n by k in the 3rd term of RHS and then switching k and j in the same term, one obtains

$$\begin{aligned} \left[\sum_{j=1}^N \hat{\mathbf{r}}_j \frac{1}{2} \sum_{\substack{k=1 \\ k \neq j}}^N \hat{V}(r_{kj}), \sum_{n=1}^N \frac{\hat{\mathbf{p}}_n^2}{2m_n} \right] &= \frac{1}{2} i\hbar \sum_{j=1}^N \frac{\hat{\mathbf{p}}_j}{m_j} \sum_{\substack{k=1 \\ k \neq j}}^N \hat{V}(r_{kj}) - \frac{1}{2} i\hbar \sum_{j=1}^N \sum_{\substack{k=1 \\ k \neq j}}^N \hat{\mathbf{r}}_j \left[\frac{\partial \hat{V}(r_{kj})}{\partial \mathbf{r}_{kj}} \cdot \frac{\hat{\mathbf{p}}_j}{2m_j} + \frac{\hat{\mathbf{p}}_j}{2m_j} \cdot \frac{\partial \hat{V}(r_{kj})}{\partial \mathbf{r}_{kj}} \right] \\ &\quad - \frac{1}{2} i\hbar \sum_{j=1}^N \sum_{\substack{k=1 \\ k \neq j}}^N \hat{\mathbf{r}}_k \left[\frac{\partial \hat{V}(r_{kj})}{\partial \mathbf{r}_{kj}} \cdot \frac{\hat{\mathbf{p}}_j}{2m_j} + \frac{\hat{\mathbf{p}}_j}{2m_j} \cdot \frac{\partial \hat{V}(r_{kj})}{\partial \mathbf{r}_{kj}} \right]. \end{aligned} \quad (\text{A8})$$

Equations (A2) and (A5) also lead to

$$\begin{aligned} \left[\sum_{j=1}^N \hat{\mathbf{r}}_j \frac{\hat{\mathbf{p}}_j^2}{2m_j}, \frac{1}{2} \sum_{k=1}^N \sum_{\substack{n=1 \\ n \neq k}}^N \hat{V}(r_{nk}) \right] &= -\frac{1}{2} i\hbar \sum_{j=1}^N \sum_{\substack{n=1 \\ n \neq j}}^N \hat{\mathbf{r}}_j \left[\frac{\partial \hat{V}(r_{jn})}{\partial \mathbf{r}_{jn}} \cdot \frac{\hat{\mathbf{p}}_j}{2m_j} + \frac{\hat{\mathbf{p}}_j}{2m_j} \cdot \frac{\partial \hat{V}(r_{jn})}{\partial \mathbf{r}_{jn}} \right] \\ &\quad + \frac{1}{2} i\hbar \sum_{j=1}^N \sum_{\substack{k=1 \\ k \neq j}}^N \hat{\mathbf{r}}_j \left[\frac{\partial \hat{V}(r_{kj})}{\partial \mathbf{r}_{kj}} \cdot \frac{\hat{\mathbf{p}}_j}{2m_j} + \frac{\hat{\mathbf{p}}_j}{2m_j} \cdot \frac{\partial \hat{V}(r_{kj})}{\partial \mathbf{r}_{kj}} \right]. \end{aligned} \quad (\text{A9})$$

Replacing n by k in the 1st term produces

$$\left[\sum_{j=1}^N \hat{\mathbf{r}}_j \frac{\hat{\mathbf{p}}_j^2}{2m_j}, \frac{1}{2} \sum_{k=1}^N \sum_{\substack{n=1 \\ n \neq k}}^N \hat{V}(r_{nk}) \right] = i\hbar \sum_{j=1}^N \sum_{\substack{k=1 \\ k \neq j}}^N \hat{\mathbf{r}}_j \left[\frac{\partial \hat{V}(r_{kj})}{\partial \mathbf{r}_{kj}} \cdot \frac{\hat{\mathbf{p}}_j}{2m_j} + \frac{\hat{\mathbf{p}}_j}{2m_j} \cdot \frac{\partial \hat{V}(r_{kj})}{\partial \mathbf{r}_{kj}} \right]. \quad (\text{A10})$$

It is trivial to show

$$\left[\sum_{j=1}^N \hat{\mathbf{r}}_j \left(\frac{\hat{\mathbf{p}}_j^2}{2m_j} + \frac{1}{2} \sum_{\substack{k=1 \\ j \neq k}}^N \hat{V}(r_{jk}) \right), \hat{H} \right] = \left[\sum_{j=1}^N \hat{\mathbf{r}}_j \frac{\hat{\mathbf{p}}_j^2}{2m_j}, \sum_{n=1}^N \frac{\hat{\mathbf{p}}_n^2}{2m_n} \right] + \left[\sum_{j=1}^N \hat{\mathbf{r}}_j \frac{\mathbf{p}_j^2}{2m_j}, \frac{1}{2} \sum_{k=1}^N \sum_{\substack{n=1 \\ n \neq k}}^N \hat{V}(r_{nk}) \right] \\ + \left[\hat{\mathbf{r}}_j \frac{1}{2} \sum_{\substack{k=1 \\ k \neq j}}^N \hat{V}(r_{kj}), \sum_{n=1}^N \frac{\hat{\mathbf{p}}_n^2}{2m_n} \right], \quad (\text{A11})$$

which leads to

$$\left[\sum_{j=1}^N \hat{\mathbf{r}}_j \left(\frac{\hat{\mathbf{p}}_j^2}{2m_j} + \frac{1}{2} \sum_{\substack{k=1 \\ j \neq k}}^N \hat{V}(r_{jk}) \right), \hat{H} \right] = i\hbar \sum_{j=1}^N \frac{\hat{\mathbf{p}}_j}{m_j} \frac{\hat{\mathbf{p}}_j^2}{2m_j} + \frac{1}{2} i\hbar \sum_{j=1}^N \sum_{\substack{k=1 \\ k \neq j}}^N \frac{\hat{\mathbf{p}}_j}{m_j} \hat{V}(r_{kj}) \\ - \frac{1}{2} i\hbar \sum_{j=1}^N \sum_{\substack{k=1 \\ k \neq j}}^N \hat{\mathbf{r}}_{kj} \left[\frac{\partial \hat{V}(r_{kj})}{\partial \mathbf{r}_{kj}} \cdot \frac{\hat{\mathbf{p}}_j}{2m_j} + \frac{\hat{\mathbf{p}}_j}{2m_j} \cdot \frac{\partial \hat{V}(r_{kj})}{\partial \mathbf{r}_{kj}} \right], \quad (\text{A12})$$

by virtue of Eqs. (A6) and (A7), and (A10). Similarly, it is straightforward to show Eq. (7) is the expression of the energy current operator $\hat{\mathbf{G}}$ (i.e., Eq. (6)).

APPENDIX B: WIGNER FUNCTION FOR OPERATOR \hat{B}

Considering operator $\hat{B} = (f(\hat{x})h(\hat{p})g(\hat{x}) + g(\hat{x})h(\hat{p})f(\hat{x}))/2$ with f, h, g real functions, one can express the Wigner function for operator \hat{B} as

$$B_w(x, p) = \int d\Delta x e^{\frac{i}{\hbar}p\Delta x} \times \left\langle x - \frac{\Delta x}{2} \left| \frac{f(\hat{x})h(\hat{p})g(\hat{x}) + g(\hat{x})h(\hat{p})f(\hat{x})}{2} \right| x + \frac{\Delta x}{2} \right\rangle. \quad (\text{B1})$$

Inserting a complete set $1 \equiv \int dp |p\rangle \langle p|$ into the RHS of Eq. (B1) gives

$$B_w(x, p) = \int d\Delta x \int d\bar{p} e^{\frac{i}{\hbar}p\Delta x} h(\bar{p}) \left\langle x - \frac{\Delta x}{2} \left| \bar{p} \right\rangle \langle \bar{p} \left| x + \frac{\Delta x}{2} \right\rangle \frac{f\left(x - \frac{\Delta x}{2}\right)g\left(x + \frac{\Delta x}{2}\right) + f\left(x + \frac{\Delta x}{2}\right)g\left(x - \frac{\Delta x}{2}\right)}{2}, \quad (\text{B2})$$

which leads to

$$B_w(x, p) = \frac{1}{2\pi\hbar} \int d\Delta x \int d\bar{p} e^{\frac{i}{\hbar}(p-\bar{p})\Delta x} h(\bar{p}) \frac{f\left(x - \frac{\Delta x}{2}\right)g\left(x + \frac{\Delta x}{2}\right) + f\left(x + \frac{\Delta x}{2}\right)g\left(x - \frac{\Delta x}{2}\right)}{2}. \quad (\text{B3})$$

Expanding the third term of the RHS of Eq. (B3) into a Tylor series of Δx , one obtains

$$B_w(x, p) = \int d\bar{p} \delta(p - \bar{p}) h(\bar{p}) f(x) g(x) + \frac{1}{2\pi\hbar} \int d\Delta x \int d\bar{p} \frac{\partial^2 \left(e^{\frac{i}{\hbar}(p-\bar{p})\Delta x} \right)}{\partial \left(\frac{i}{\hbar}\bar{p} \right)^2} \\ \times h(\bar{p}) \frac{f''(x)g(x) + f(x)g''(x) - 2f'(x)g'(x)}{8} + \dots. \quad (\text{B4})$$

It is then easy to show

$$B_w(x, p) = h(p) f(x) g(x) - \hbar^2 h''(p) \frac{f''(x)g(x) + f(x)g''(x) - 2f'(x)g'(x)}{8} + \dots, \quad (\text{B5})$$

after integrating by parts in the RHS of Eq. (B4). One, therefore, proves

$$B_w(x, p) = f(x) g(x) p, \quad (\text{B6})$$

for $h(\hat{p}) = \hat{p}$. That is, $B_w(x, p)$ is simply the classical function itself. Although the proof is shown for 1-dim systems, it is straightforward to extend it for multi-dimensional systems.

- ¹W. H. Miller, *Adv. Chem. Phys.* **25**, 69 (1974).
- ²W. H. Miller, *Adv. Chem. Phys.* **30**, 77 (1975).
- ³W. H. Miller, *Proc. Natl. Acad. Sci. U.S.A.* **102**, 6660 (2005).
- ⁴H. Wang, X. Sun, and W. H. Miller, *J. Chem. Phys.* **108**, 9726 (1998).
- ⁵J. Liu and W. H. Miller, *J. Chem. Phys.* **131**, 074113 (2009).
- ⁶Q. Shi and E. Geva, *J. Chem. Phys.* **118**, 8173 (2003).
- ⁷X. Sun, H. Wang, and W. H. Miller, *J. Chem. Phys.* **109**, 7064 (1998).
- ⁸T. Yamamoto and W. H. Miller, *J. Chem. Phys.* **118**, 2135 (2003).
- ⁹J. Liu and W. H. Miller, *J. Chem. Phys.* **125**, 224104 (2006).
- ¹⁰J. Liu and W. H. Miller, *J. Chem. Phys.* **126**, 234110 (2007).
- ¹¹J. Liu and W. H. Miller, *J. Chem. Phys.* **127**, 114506 (2007).
- ¹²J. Liu and W. H. Miller, *J. Chem. Phys.* **128**, 144511 (2008).
- ¹³J. Liu and W. H. Miller, *J. Chem. Phys.* **129**, 124111 (2008).
- ¹⁴Q. Shi and E. Geva, *J. Phys. Chem. A* **107**, 9059 (2003).
- ¹⁵Q. Shi and E. Geva, *J. Phys. Chem. A* **107**, 9070 (2003).
- ¹⁶B. J. Ka and E. Geva, *J. Phys. Chem. A* **110**, 9555 (2006).
- ¹⁷J. Liu, W. H. Miller, F. Paesani, W. Zhang, and D. Case, *J. Chem. Phys.* **131**, 164509 (2009).
- ¹⁸J. A. Poulsen, G. Nyman, and P. J. Rossky, *J. Phys. Chem. B* **108**, 19799 (2004).
- ¹⁹J. A. Poulsen, G. Nyman, and P. J. Rossky, *Proc. Natl. Acad. Sci. U.S.A.* **102**, 6709 (2005).
- ²⁰J. A. Poulsen, J. Scheers, G. Nyman, and P. J. Rossky, *Phys. Rev. B* **75**, 224505 (2007).
- ²¹T. D. Hone, J. A. Poulsen, P. J. Rossky, and D. E. Manolopoulos, *J. Phys. Chem. B* **112**, 294 (2008).
- ²²J. Shao and N. Makri, *J. Phys. Chem. A* **103**, 7753 (1999).
- ²³J. Shao and N. Makri, *J. Phys. Chem. A* **103**, 9479 (1999).
- ²⁴N. Makri, A. Nakayama, and N. Wright, *J. Theor. Comput. Chem.* **3**, 391 (2004).
- ²⁵J. Liu and N. Makri, *Chem. Phys.* **322**, 23 (2006).
- ²⁶J. Liu, A. Nakayama, and N. Makri, *Mol. Phys.* **104**, 1267 (2006).
- ²⁷A. Nakayama and N. Makri, *Proc. Natl. Acad. Sci. U.S.A.* **102**, 4230 (2005).
- ²⁸W. H. Miller, *J. Chem. Phys.* **125**, 132305 (2006).
- ²⁹B. J. Alder, D. M. Gass, and T. E. Wainwright, *J. Chem. Phys.* **53**, 3813 (1970).
- ³⁰D. A. McQuarrie, *Statistical Mechanics* (University Science Books, Sausalito, CA, 2000).
- ³¹R. Zwanzig, *Annu. Rev. Phys. Chem.* **16**, 67 (1965).
- ³²B. J. Berne and G. D. Harp, *Adv. Chem. Phys.* **17**, 63 (1970).
- ³³R. Kubo, M. Toda, and N. Hashitsume, *Statistical Physics II: Nonequilibrium Statistical Mechanics*, 2nd ed. (Springer-Verlag, Heidelberg, 1991).
- ³⁴L. P. Kadanoff and P. C. Martin, *Ann. Phys.* **24**, 419 (1963).
- ³⁵H. Mori, *Phys. Rev.* **112**, 1829 (1958).
- ³⁶M. S. Green, *J. Chem. Phys.* **22**, 398 (1954).
- ³⁷R. Kubo, *J. Phys. Soc. Jpn.* **12**, 570 (1957).
- ³⁸E. Helfand, *Phys. Rev.* **119**, 1 (1960).
- ³⁹J. J. Erpenbeck, *Phys. Rev. E* **51**, 4296 (1995).
- ⁴⁰M. S. Green, *J. Chem. Phys.* **20**, 1281 (1952).
- ⁴¹Y. Yonetani and K. Kinugawa, *J. Chem. Phys.* **120**, 10624 (2004).
- ⁴²J. Liu, W. H. Miller, G. S. Fanourgakis, S. S. Xantheas, I. Sho, and S. Saito, (submitted).
- ⁴³E. P. Wigner, *Phys. Rev.* **40**, 749 (1932).
- ⁴⁴E. J. Wigner, *Trans. Faraday Soc.* **34**, 29 (1938).
- ⁴⁵E. J. Heller, *J. Chem. Phys.* **65**, 1289 (1976).
- ⁴⁶H. W. Lee and M. O. Scully, *J. Chem. Phys.* **73**, 2238 (1980).
- ⁴⁷E. Pollak and J. L. Liao, *J. Chem. Phys.* **108**, 2733 (1998).
- ⁴⁸J. A. Poulsen, G. Nyman, and P. J. Rossky, *J. Chem. Phys.* **119**, 12179 (2003).
- ⁴⁹J. Liu and W. H. Miller, *J. Chem. Phys.* **134**, 104102 (2011).
- ⁵⁰J. Liu and W. H. Miller, *J. Chem. Phys.* **134**, 104101 (2011).
- ⁵¹This further simplifying approximation is fine for the thermal conductivity because it is a transport property (i.e., zero-frequency mode) and it should not matter whether we follow the path integral bead or the centroid. However, we do not recommend it when the whole spectrum of the correlation function is needed. The local Gaussian approximation (Ref. 5) or several other approximations will be more appropriate.
- ⁵²R. Eggenberger, S. Gerber, H. Huber, D. Searles, and M. Welker, *Mol. Phys.* **76**, 1213 (1992).
- ⁵³N. B. Vargaftik, *Tables on the Thermophysical Properties of Liquids and Gases: in Normal and Dissociated States*, (Hemisphere, New York, 1975).
- ⁵⁴*Thermodynamic Properties of Neon, Argon, Krypton, and Xenon*, edited by V. A. Rabinovich, A. A. Vasserman, V. I. Nedostup, and L. S. Veksler (Springer-Verlag, Berlin, 1988).
- ⁵⁵I. F. Silvera and V. V. Goldman, *J. Chem. Phys.* **69**, 4209 (1978).
- ⁵⁶D. J. Scharf, G. J. Martyna, and M. L. Klein, *Low Temp. Phys.* **19**, 364 (1993).
- ⁵⁷A. Nakayama and N. Makri, *J. Chem. Phys.* **119**, 8592 (2003).
- ⁵⁸B. I. Verkin, *Handbook of Properties of Condensed Phases of Hydrogen and Oxygen*, Revised and Augmented English ed. (Hemisphere, New York, 1990).
- ⁵⁹H. M. Roder and D. E. Diller, *J. Chem. Phys.* **52**, 5928 (1970).
- ⁶⁰J. W. Leachman, R. T. Jacobsen, S. G. Penoncello, and M. L. Huber, *Int. J. Thermophys.* **28**, 773 (2007).
- ⁶¹R. A. Aziz, M. J. Slaman, A. Koide, A. R. Allnatt, and W. J. Meath, *Mol. Phys.* **77**, 321 (1992).
- ⁶²R. J. Donnelly and C. F. Barenghi, *The Observed Properties of Liquid Helium at the Saturated Vapor Pressure* (<http://pages.uoregon.edu/rjd/vapor1.htm>).
- ⁶³V. N. Peshkov, *Soviet Physics Uspekhi-Ussr* **11**, 209 (1968).
- ⁶⁴J. F. Kerrisk, "The Thermal Conductivity of Liquid Helium 4 and Liquid Helium 3," Ph.D. dissertation, The University of New Mexico, 1968.
- ⁶⁵D. M. Ceperley, *Rev. Mod. Phys.* **67**, 279 (1995).
- ⁶⁶The agreement with experiment for liquid neon, however, is most likely fortuitous, since the uncertainty in the pair potential as well as the many-body contribution to the potential at liquid densities could lead to larger errors to the thermal conductivity than the quantum corrections. For instance, as we have already tested and as shown (for the classical simulation) in Ref. 52, the thermal conductivity for the conventional Lennard-Jones potential for liquid neon is 10%–20% different from that for the *ab initio*-based potential presented in the current manuscript.
- ⁶⁷A. J. H. McGaughey and M. Kaviany, *Int. J. Heat Mass Transfer* **47**, 1783 (2004).
- ⁶⁸P. Keblinski, S. R. Phillpot, S. U. S. Choi, and J. A. Eastman, *Int. J. Heat Mass Transfer* **45**, 855 (2002).
- ⁶⁹J. Liu, *J. Chem. Phys.* **134**, 194110 (2011).